

UC Irvine

UC Irvine Previously Published Works

Title

Investigating evidence for different black hole accretion modes since redshift $z \sim 1$

Permalink

<https://escholarship.org/uc/item/5148516g>

Journal

Monthly Notices of the Royal Astronomical Society, 440(1)

ISSN

0035-8711

Authors

Georgakakis, A
Pérez-González, PG
Fanidakis, N
et al.

Publication Date

2014-05-01

DOI

10.1093/mnras/stu236

Peer reviewed

Investigating evidence for different black hole accretion modes since redshift $z \sim 1$

A. Georgakakis^{1,2}, P. G. Pérez-González^{3,4}, N. Fanidakis⁵, M. Salvato¹, J. Aird⁶,
H. Messias⁷, J. M. Lotz⁸, G. Barro⁹, Li-Ting Hsu¹, K. Nandra¹, D. Rosario¹,
M. C. Cooper¹⁰, D. D. Kocevski¹¹, J. A. Newman¹²

¹*Department of Physics and Astronomy Planck Institut für Extraterrestrische Physik, Giessenbachstraße, 85748 Garching, Germany*

²*IAASARS, National Observatory of Athens, GR-15236 Penteli, Greece*

³*Departamento de Astrofísica, Facultad de CC. Físicas, Universidad Complutense de Madrid, E-28040 Madrid, Spain*

⁴*Steward Observatory, The University of Arizona, 933 N. Cherry Ave., Tucson, AZ 85721, USA*

⁵*Max Planck Institut für Astronomie, Königstuhl 17, D-69117, Heidelberg, Germany*

⁶*Extragalactic & Cosmology Group, Rochester Building, Department of Physics, University of Durham, Science Laboratories South Road Durham DH1 3LE.*

⁷*Departamento de Astronomía, Av. Esteban Iturra 6to piso, Facultad de Ciencias Físicas y Matemáticas, Universidad de Concepción, Chile.*

⁸*Space Telescope Science Institute, 3700 San Martin Drive, Baltimore, MD 21218, USA*

⁹*UCO/Lick Observatory, University of California, Santa Cruz, 1156 High Street, Santa Cruz, CA 95064*

¹⁰*Center for Galaxy Evolution, Department of Physics and Astronomy, University of California, Irvine, 4129 Frederick Reines Hall Irvine, CA 92697 USA*

¹¹*University of Kentucky, Department of Physics and Astronomy, 177 Chemistry-Physics Building, Lexington, KY 40506-0055, USA*

¹²*Department of Physics and Astronomy & Pittsburgh Particle Physics, Astrophysics and Cosmology Center (PITT PACC), University of Pittsburgh, Pittsburgh, PA 15260, USA*

12 February 2014

ABSTRACT

Chandra data in the COSMOS, AEGIS-XD and 4 Ms Chandra Deep Field South are combined with multiwavelength photometry available in those fields to determine the rest-frame $U - V$ vs $V - J$ colours of X-ray AGN hosts in the redshift intervals $0.1 < z < 0.6$ (mean $\bar{z} = 0.40$) and $0.6 < z < 1.2$ (mean $\bar{z} = 0.85$). This combination of colours provides an effective and least model-dependent means of separating quiescent from star-forming, including dust reddened, galaxies. Morphological information emphasises differences between AGN populations split by their $U - V$ vs $V - J$ colours. AGN in quiescent galaxies consist almost exclusively of bulges, while star-forming hosts are equally split between early and late-type hosts. The position of AGN hosts on the $U - V$ vs $V - J$ diagram is then used to set limits on the accretion density of the Universe associated with evolved and star-forming systems independent of dust induced biases. It is found that most of the black hole growth at $z \approx 0.40$ and 0.85 is associated with star-forming hosts. Nevertheless, a non-negligible fraction of the X-ray luminosity density, about 15-20%, at both $\bar{z} = 0.40$ and 0.85 , is taking place in galaxies in the quiescent region of the $U - V$ vs $V - J$ diagram. For the low-redshift subsample, $0.1 < z < 0.6$, we also find tentative evidence, significant at the 2σ level, that AGN split by their $U - V$ and $V - J$ colours have different Eddington ratio distributions. AGN in blue star-forming hosts dominate at relatively high Eddington ratios. In contrast, AGN in red quiescent hosts become increasingly important as a fraction of the total population toward low Eddington ratios. At higher redshift, $z > 0.6$, such differences are significant at the 2σ level only for sources with Eddington ratios $\gtrsim 10^{-3}$. These findings are consistent with scenarios in which diverse accretion modes are responsible for the build-up of supermassive black holes at the centres of galaxies. We compare these results with the predictions of the GALFORM semi-analytic model for the cosmological evolution of AGN and galaxies. This model postulates two black hole fuelling modes, the first is linked to star-formation events and the second takes place in passive galaxies. GALFORM predicts that a substantial fraction of the black hole growth at $z < 1$ is associated with quiescent galaxies, in apparent conflict with the observations. Relaxing the strong assumption of the model that passive AGN hosts have zero star-formation rate could bring those predictions in better agreement with the data.

Key words: galaxies: active – galaxies: Seyferts – X-rays: diffuse background

1 INTRODUCTION

In recent years observational data established that supermassive black holes (SMBHs) are nearly ubiquitous in local spheroids (e.g. Magorrian et al. 1998). Moreover, correlations were discovered between the masses of those black holes and the stellar component of the bulges in which they reside (e.g. Kormendy & Ho 2013, and references therein). These empirical correlations have been combined with large galaxy surveys to place tight constraints on the mass function of dormant SMBHs in the nearby Universe (e.g. Kelly & Merloni 2012). What remains unclear however, is how the relic SMBHs we observe in nearby galaxies grow their mass across cosmic time. One way to approach this question is to conduct population studies of the galaxies that host active SMBHs at different redshifts. The properties (e.g. morphology, environment) of the galaxies with an Active Galactic Nucleus (AGN) provide information on the physical conditions on large (kpc to Mpc) scales which may be relevant to the fuelling of the SMBH.

Morphological studies for example, find that X-ray AGN hosts in the redshift range $z \approx 0.5 - 2$ have diverse morphologies (spiral, elliptical, disturbed) with a relative mix that is similar to that of mass-matched non-AGN galaxy samples (e.g. Georgakakis et al. 2009; Cisternas et al. 2011; Kocevski et al. 2012). This suggests that major mergers, which are expected to be associated with morphologically disturbed systems, cannot be the only channel for growing black holes at the centres of galaxies. Other mechanisms, e.g. minor interactions or secular processes, must also contribute to the accretion density of the Universe. This conclusion is also supported by large scale structure studies, which estimate mean dark matter halo masses for X-ray AGN in the range $\log(M/M_\odot) \approx 12.5 - 13.5$. This mass interval is larger than expected if black hole accretion is triggered by major mergers only (e.g. Allevato et al. 2011; Mountrichas & Georgakakis 2012; Mountrichas et al. 2013). Recent work by Fanidakis et al. (2013) indeed shows that the clustering of X-ray AGN at $z \lesssim 1.5$ is consistent with two channels for growing SMBHs. The first is associated with star-formation events in the host galaxy and the second is related to quiescent galaxies in massive halos. In the modelling of Fanidakis et al. (2013) star-formation is a proxy to cold gas availability. Galaxies with abundant cold gas supplies can form stars and grow their central black holes at a high rate. In contrast, the SMBHs of evolved galaxies that are devoid of cold gas can only grow slowly via the accretion of hot gas from a quasi-static atmosphere. Evidence for a dichotomy in the accretion rate distribution of narrow optical emission-line AGN based on the star-formation history of their hosts is reported at low redshifts (Kauffmann & Heckman 2009). This finding further supports claims for diverse AGN fuelling modes and suggests that the star-formation properties of AGN hosts hold important information on the physical conditions under which black holes at the centres of galaxies build-up their mass.

The evidence above has motivated efforts to understand the star-formation level of AGN hosts at higher redshift to explore how black holes are fuelled as a function of cosmic time. Population studies have established that the build-up of black holes and galaxies are related in a statistical sense when integrated in a cosmological volume. The star-formation rate density (Hopkins & Beacom 2006) and the accretion luminosity density (Aird et al. 2010) follow very similar evolution patterns with redshift. There is also evidence that the cosmological evolution of the AGN space density is related to the increase with redshift of the average specific star-formation rate (star-formation rate per unit stellar mass) of galaxies (e.g. Georgakakis et al. 2011). Far-IR/sub-mm observations with

Herschel extended measurements of the star-formation rate of individual AGN to high redshift and also bright accretion luminosities (e.g. luminous QSOs) where other indicators (e.g. optical spectral features, broad-band colours) become unreliable. Although it does not appear that there is a one-to-one correspondence between the level of star-formation and the accretion power (Mullaney et al. 2012; Rosario et al. 2012), X-ray AGN are on average associated with galaxies on the main star-formation sequence (Santini et al. 2012; Mullaney et al. 2012; Rovilos et al. 2012; Rosario et al. 2013).

In a typical Herschel far-IR/sub-mm survey field however, a substantial fraction of the AGN population lies below the formal detection limit. Stacking the far-IR/sub-mm counts at the positions of X-ray sources is used extensively to reach deeper flux limits and explore the star-formation properties of the entire population. Although valuable, this approach has the limitation that it estimates only the mean far-IR/sub-mm properties of AGN hosts and provides only limited information on the underlying distribution. A small sub-population of AGN not associated with high specific star-formation rate events is likely to be averaged out in far-IR/sub-mm stacking studies. Optical observations for example, show that a large fraction of the X-ray AGN hosts at $z \lesssim 1$ lie in the red sequence of the colour-magnitude diagram (e.g. Hickox et al. 2009; Georgakakis et al. 2011), which includes a large fraction of passive galaxies. Although dust can redden the broad-band colours of galaxies, it cannot account for the entire population of AGN hosts on the red sequence of the colour magnitude diagram. Cardamone et al. (2010b) for example, find evidence for a bi-modal $U - V$ rest-frame colour distribution for AGN hosts at $z \approx 1$, once the impact of dust is accounted for via fitting templates to the observed spectral energy distributions. Mignoli et al. (2004) argue that obscured X-ray selected QSO hosts at $z \approx 1 - 2$ have rest-frame optical light profiles that follow the de vaucouleurs law. This is interpreted as evidence that a large fraction of the obscured QSO population at $z \approx 1 - 2$ is hosted by bulge-dominated galaxies, possibly quiescent ellipticals (but see Hutchings et al. 2002).

In this paper we place limits on the fraction of the accretion density of the Universe associated with quiescent, low specific star-formation galaxies in the redshift range 0.1–1.2. X-ray data are used to select AGN and their rest-frame broad-band colours are adopted as the least model-dependent method to discriminate between evolved and actively star-forming hosts. Dust reddening issues are mitigated by placing X-ray AGN hosts on the $U - V$ vs $V - J$ (UVJ) colour-colour diagram (Williams et al. 2009; Patel et al. 2012). This combination of colours is least sensitive to dust extinction and has been shown to be effective in separating early-type, low-specific star-formation rate galaxies from actively star-forming, including dust-reddened systems (Williams et al. 2009). Throughout this paper we adopt $H_0 = 70 \text{ km s}^{-1} \text{ Mpc}^{-1}$, $\Omega_M = 0.3$ and $\Omega_\Lambda = 0.7$.

2 X-RAY AGN SAMPLE

We combine data from X-ray surveys with different characteristics in terms of area coverage and X-ray depth. These are the 4 Ms Chandra Deep Field South (CDFs; Xue et al. 2011), the Chandra 800 ks survey of the AEGIS field (AEGIS-XD; Nandra et al. in prep) and the Chandra survey of the COSMOS field (C-COSMOS, Elvis et al. 2009). These samples provide sufficient coverage of the $L_X - z$ plane to explore the evolution of the properties of X-ray AGN hosts since $z \approx 1$.

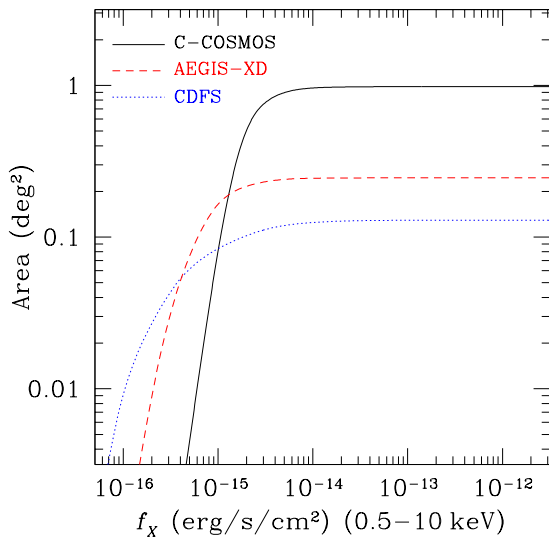


Figure 1. Sensitivity curves in the 0.5–10 keV energy band for the CDFS, AEGIS-XD and C-COSMOS fields.

The Chandra observations of the CDFS, AEGIS-XD and C-COSMOS were analysed in a homogeneous way by applying the reduction and source detection methodology described by Laird et al. (2009). The motivation for this is to have a homogeneous and well characterised X-ray selection function across the three fields, which is advantageous when studying the statistical properties of the X-ray detected population. A total of 569, 937 and 1584 X-ray sources are detected in the CDFS, AEGIS-XD and C-COSMOS, respectively, in at least one of the soft (0.5–2 keV), hard (2–7 keV), full (0.5–7 keV) or ultra-hard (5–7 keV) spectral bands to the Poisson false detection threshold of 4×10^{-6} (see Laird et al. 2009 for details). The number of X-ray detections in the CDFS and C-COSMOS is smaller than that in the catalogues published by Xue et al. (2011) and Elvis et al. (2009), respectively. This is because of the lower detection threshold adopted in those studies. The optical identification of the X-ray sources was based on the Likelihood Ratio method (Sutherland & Saunders 1992). The CDFS X-ray sources were cross-matched with the MUSYC optical photometric catalogue (Cardamone et al. 2010a). In the case of the AEGIS-XD we used the IRAC-3.6 μm selected multi-wavelength photometric catalogue provided by the Rainbow Cosmological Surveys Database (Pérez-González et al. 2008; Barro et al. 2011b,a). The identification of C-COSMOS X-ray sources used the *I*-band selected optical sample of Capak et al. (2007) and the IRAC-3.6 μm catalogue of Sanders et al. (2007).

Extensive spectroscopic campaigns have been carried out in the fields of choice. In the CDFS we used the spectroscopic redshifts compiled by Cardamone et al. (2010a) as part of the MUSYC multiwavelength catalogue release. Spectroscopic redshift measurements of X-ray sources in the AEGIS field are primarily from the DEEP2 (Newman et al. 2012) and DEEP3 galaxy redshift surveys (Cooper et al. 2011, 2012) as well as observations carried out at the MMT using the Hectospec fibre spectrograph (Coil et al. 2009). Redshifts in the C-COSMOS are from the public releases of the VIMOS/zCOSMOS bright project (Lilly et al. 2009) and the Magellan/IMACS observation campaigns (Trump et al. 2009), as

well as the compilation of redshifts for X-ray sources presented by Brusa et al. (2010).

We select X-ray sources with $\mathcal{R} < 24$ mag, where \mathcal{R} stands for either the MUSYC *R*-band in the case of the CDFS, the r' filter of the CFHT (Canada-France-Hawaii Telescope) Megaprime camera for the AEGIS-XD or the Subaru Suprime-Cam instrument r^+ band in the case of C-COSMOS. At these magnitude limits the spectroscopic identification rate of the CDFS, AEGIS-XD, and C-COSMOS X-ray sources is 78 (176/224), 70 (288/414) and 75 (726/962) per cent, respectively (see Table 1). We also limit the sample to X-ray sources with spectroscopic redshift measurements in the range 0.1 – 1.2 (see Table 1 for the total number of sources). X-ray sources brighter than $\mathcal{R} = 24$ mag without spectroscopic redshift measurements are used only indirectly in the analysis. The photometric redshift probability distributions (PDZ) of those sources are integrated to estimate corrections for spectroscopic incompleteness in the calculation of the space density of AGN (see section 4). The X-ray AGN photometric redshifts and PDZs are from Salvato et al. (2011) for C-COSMOS and Nandra et al. (in prep) for the AEGIS-XD. The methodology described in those publications have also been applied to the MUSYC photometry to determine PDZs for the CDFS X-ray sources. A by-product of the photometric redshift determination is the characterisation of the Spectral Energy Distribution (SED) of X-ray AGN, e.g. host galaxy type, level of optical extinction, level of the AGN component relative to the underlying host galaxy. The latter information is used in later sections to identify sources for which the AGN radiation likely contaminates the host galaxy light.

The CDFS, AEGIS-XD and C-COSMOS spectroscopic X-ray AGN samples are split into two redshift bins, 0.1–0.6 and 0.6–1.2, with medians 0.40 and 0.85, respectively. We choose to select sources in the 0.5–7 keV spectral band for both redshift subsamples. The total number of X-ray sources in each field is shown in Table 1. The X-ray sensitivity curves are estimated by extrapolating the background counts and exposure maps in the 0.5–7 keV band to the limiting flux of a source in the 0.5–10 keV energy range. The resulting X-ray sensitivity curves are plotted in Figure 1 for the 3 survey fields used in the analysis.

High resolution imaging observations from the Hubble Space Telescope (HST) are also used to explore the morphology of the host galaxies of X-ray sources. The Advanced Camera for Surveys (ACS) aboard HST has surveyed the central most sensitive part of the CDFS in four passbands, F435W, F606W, F775W and F850LP, with corresponding exposure times 7200, 5450, 7028 and 18200 s, respectively. The survey setup, data reduction and source detection is described by Giavalisco et al. (2004). The estimated 10σ point source limiting magnitude in the F775W filter is about 27 mag. About 75% of the 4Ms CDFS X-ray sources overlap with the HST survey region. The AEGIS-XD field also has HST/ACS imaging in the F606W (2260 s) and F814W (2100 s) filters (Lotz et al. 2008). These observations cover a subregion of the AEGIS-XD that includes about 65% of the X-ray sources. The 5 sigma limiting magnitudes for a point source are $V_{F606W} = 28.14$ (AB) and $I_{F814W} = 27.52$ (AB). The HST surveyed the COSMOS field with the ACS in the F814W filter (Koekemoer et al. 2007). The median exposure time across the field is 2028 s, which yields a limiting point-source depth of 27.2 mag (5σ).

Table 1. X-ray AGN and galaxy samples

field	0.5-7 keV selected sample	$\mathcal{R} < 24$ mag sample	z -spec sample	$0.1 < z < 0.6$ sample	$0.6 < z < 1.2$ sample
CDFS	490	224	176	45 (1)	87 (10)
AEGIS-XD	859	414	288	55 (7)	121 (18)
C-COSMOS	1477	962	726	138 (16)	282 (65)

The columns are: (1) field name; (2) total number of X-ray sources detected in the 0.5-7 keV (full) band; (3) total number of full-band selected sources with $\mathcal{R} < 24$ mag, where \mathcal{R} stands for either the MUSYC R -band (CDFS), the r' filter of the CFHT Megaprime camera (AEGIS-XD) or the Subaru Suprime-Cam instrument r^+ band (C-COSMOS); (4) number of full-band selected sources with $\mathcal{R} < 24$ mag and secure spectroscopic redshift measurements; (5) the same as in column 4 for the redshift interval 0.1–0.6. The numbers in the the parentheses correspond to X-ray AGN with SEDs that are best-fit by the Seyfert or QSO hybrid templates of Salvato et al. (2009, 2011). For these sources the optical light is contaminated by AGN emission and is therefore not representative of the underlying stellar population. They are exclude from the analysis when studying the AGN host galaxy properties (e.g. stellar mass, optical/near-IR colours); (6) the same as column 5 for the redshift interval 0.6-1.2.

3 REST-FRAME PROPERTIES

This section describes how the rest-frame colours, X-ray luminosities in the 2-10 keV band and absorbing column densities, N_H , of X-ray AGN are determined.

The KCORRECT version 4.2 routines developed by Blanton & Roweis (2007) are used to fit templates to the optical photometry of X-ray sources and estimate rest-frame colours in the AB system. Rest frame magnitudes are estimated in the Bessell (1990) U and B passbands and the 2MASS- J filter without any atmospheric corrections or detector response included. The input photometry to KCORRECT was different for each field. In the case of the CDFS we used the MUSYC $UBVRIZJHK$ broad-band photometry (Cardamone et al. 2010a). For AEGIS-XD the CFHT $ugriz$ and Palomar WIRC (Wide-field Infrared Camera) JK (Bundy et al. 2006) photometry was employed. In C-COSMOS fluxes in the CFHT u^* , SUBARU $Vg^+r^+i^+z^+$ (Capak et al. 2007), UKIRT WFCAM J (McCracken et al. 2010) and CFHT WIRCAM K_s (Capak et al. 2007) filters were provided to KCORRECT. When estimating rest-frame colours we attempt to minimise k -corrections, which unavoidably depend on the adopted set of model Spectral Energy Distributions. The rest-frame magnitude of a source in a particular filter, X , is estimated from the photometry in the waveband that has effective wavelength at the rest-frame of the source close to that of the filter X . Sources are split into two broad redshift bins, 0.1-0.6 and 0.6-1.2. The observed photometric bands used to determine rest frame UVJ magnitudes for the sources in each redshift bin are listed in Table 2.

The intrinsic column density, N_H , of individual X-ray AGN is determined from the hardness ratios between the soft (0.5-2 keV) and the hard (2-7 keV) X-ray bands assuming an intrinsic power-law X-ray spectrum with index $\Gamma = 1.9$ (e.g. Nandra & Pounds 1994). The derived column densities are then used to convert the count-rates in the 0.5-7 keV band to rest-frame 2-10 keV luminosity, $L_X(2 - 10 \text{ keV})$. We limit the sample to sources brighter than $L_X(2 - 10 \text{ keV}) = 10^{41} \text{ erg s}^{-1}$. Contamination by non-AGN at faint luminosities is a potential source of bias. Normal galaxy candidates are selected to have $L_X(2 - 10 \text{ keV}) < 10^{42} \text{ erg s}^{-1}$, $\log N_H < 22 \text{ (cm}^{-2}\text{)}$ and $f_X/f_{\mathcal{R}} < -1.5$, where $f_{\mathcal{R}}$ is the optical flux in the \mathcal{R} -band filter of each survey field. Variants of these selection criteria are often used to identify normal galaxies at X-rays (e.g. Georgakakis et al. 2007). A total of 53 galaxy candidates are identified among the spectroscopic X-ray selected sample listed in Table 1. These sources are removed from the analysis.

Stellar masses of AGN host galaxies in the 3 fields are calculated using the methods presented in Pérez-González et al. (2008)

and Barro et al. (2011b,a). The observed SED of each source is fit with a large set of templates based on PEGASE version 1 (Fioc & Rocca-Volmerange 1997) tau-models (running from a single stellar population to continuous SFR) and assuming a Salpeter Initial Mass Function (IMF; stellar mass range 0.1 – 100 M_{\odot}), different metallicities and the Calzetti et al. (2000) extinction law. We do not measure stellar masses for X-ray sources for which the SED fitting process described in Section 2 suggests a significant AGN component that could contaminate the host galaxy emission. These are sources fit with any of the Seyfert or QSO hybrid templates of Salvato et al. (2009, 2011). The number of these X-ray AGN are listed in Table 1.

4 THE AGN X-RAY LUMINOSITY FUNCTION

The X-ray luminosity function of AGN is derived using the standard non-parametric $1/V_{\text{max}}$ method (Schmidt 1968). In this calculation we take into account the X-ray selection function, the optical magnitude limit of different samples and the spectroscopic identification incompleteness. The XLF in logarithmic bins is estimated by the relation

$$\phi(L_X, z) dL_X = \sum_i \frac{w_i}{V_{\text{max},i}}, \quad (1)$$

where w_i is the weight applied to each spectroscopically identified source i to correct for the spectroscopic incompleteness (see below). $V_{\text{max},i}$ is the maximum comoving volume for which the source i satisfies the sample selection criteria, i.e. redshift range, apparent optical magnitude limit and X-ray flux limit. $V_{\text{max},i}$ depends on X-ray luminosity, absolute optical magnitude, redshift as well as the overall shape of the optical and X-ray SED

$$V_{\text{max},i} = \frac{c}{H_0} \int_{z_1}^{z_2} \Omega(L_X, N_H, z) \frac{dV}{dz} dz dL, \quad (2)$$

where dV/dz is the volume element per redshift interval dz . The integration limits are $z_1 = z_L$ and $z_2 = \min(z_{\text{optical}}, z_U)$, where we define z_L, z_U the lower and upper redshift limits applied to the sample and z_{optical} is the redshift at which the source becomes fainter than the survey optical magnitude limit. $\Omega(L_X, N_H, z)$ is the solid angle of the X-ray survey available to a source with luminosity L_X and column density N_H at a redshift z (corresponding to a flux f_X on the X-ray sensitivity curve). The uncertainty at a given luminosity or mass bin is

$$\delta\phi^2 = \sum_i \left(\frac{w_i}{V_{\text{max},i}} \right)^2. \quad (3)$$

Table 2. Observed to rest-frame photometry

rest-frame filter	Observed band used to estimate rest-frame magnitudes for each field and redshift sub-sample					
	CDFS		AEGIS-XD		C-COSMOS	
	$0.1 < z < 0.6$	$0.6 < z < 1.2$	$0.1 < z < 0.6$	$0.6 < z < 1.2$	$0.1 < z < 0.6$	$0.6 < z < 1.2$
Johnson U	MUSYC V	MUSYC R	CFHT g	CFHT r	Subaru g^+	Subaru r^+
Johnson V	MUSYC I	MUSYC z	CFHT i	CFHT z	Subaru i^+	Subaru z^+
2MASS J	MUSYC H	MUSYC K	WIRC K	WIRC K	WIRCAM K_s	WIRCAM K_s

Listed are the observed bands in each field that are used to estimate rest-frame UVJ magnitudes. The sources are split into two broad redshift bins. At the mean redshift of each bin the listed observed bands have rest-frame effective wavelengths that are close to those of the U , V or J filters. For the $0.1 < z < 0.6$ subsamples the observed H -band photometry is best-suited for the determination of rest-frame J -band magnitudes. However, H -band photometry is not available in the AEGIS-XD and C-COSMOS fields. We therefore choose to use the K -band photometry in those fields to determine rest-frame J band magnitudes.

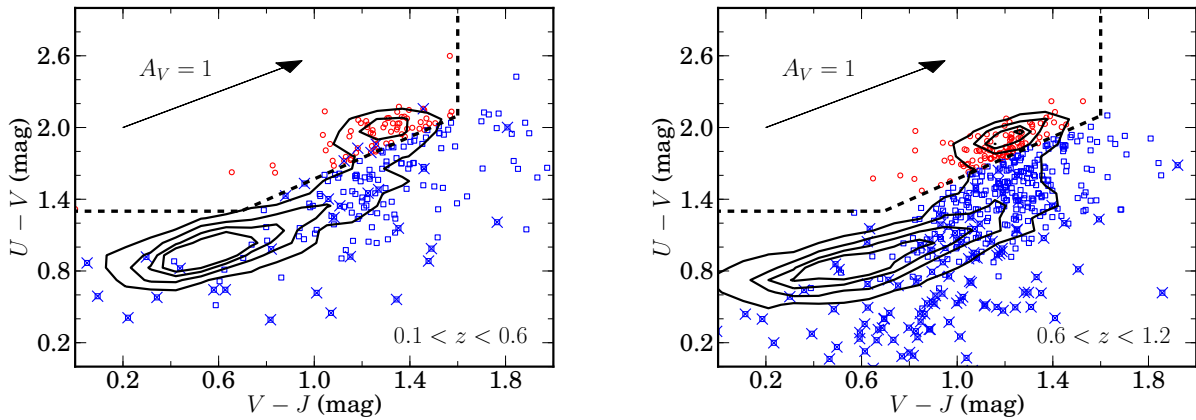


Figure 2. $U - V$ vs $V - J$ diagram of X-ray AGN (coloured symbols) and galaxies (black contours). The galaxy sample in both panels consists of sources with secure redshifts obtained as part of the large spectroscopic follow-up campaigns in the CDFS, AEGIS-XD and C-COSMOS fields, e.g. DEEP2, DEEP3 and the VIMOS/zCOSMOS bright project. The different contour levels correspond to 30, 60, 90 and 120 galaxies within bins of size 0.1 mag. The dashed lines correspond to $U - V = 0.88(V - J) + 0.69$, $U - V > 1.3$, $V - J < 1.6$ (Williams et al. 2009). In both panels galaxies are distributed into two distinct populations, i.e. quiescent and star-forming. The wedge, as defined above, marks the transition region between these two galaxy populations. The arrow shows the reddening vector with $A_V = 1$ for the Calzetti et al. (2000) law. This is parallel to the quiescent galaxy selection wedge. Dusty star-forming galaxies are therefore separated from quiescent systems. Red circles are X-ray AGN in the quiescent region of the UVJ diagram. Blue squares are X-ray in the star-forming part of the colour-colour space. Crosses on top of an X-ray AGN mark sources for which AGN radiation contaminates the underlying host galaxy continuum. The rest-frame colours of those sources are therefore not representative of their hosts.

The conversion of the absolute to apparent optical magnitude in the $1/V_{\max}$ calculation uses the optical k -corrections determined by the KCORRECT version 4.2 routines (Blanton & Roweis 2007). The model that best fits the optical photometric data of a source is also used to estimate k -corrections for the same source at different redshifts. In the case of the XLF, the intrinsic N_H of individual X-ray sources is taken into account in the $1/V_{\max}$ estimation. The X-ray k -corrections are calculated by adopting an absorbed power-law spectral energy distribution with $\Gamma = 1.9$ and photoelectric absorption cross sections as described by Morrison & McCammon (1983) for solar metallicity.

The weight w_i is estimated following a methodology similar to that described by Lin et al. (1999) and Willmer et al. (2006). For each X-ray source, i , in the sample we estimate the probability P_i that it lies within the redshift interval of interest $z_L < z < z_U$ (e.g. $0.6 < z < 1.2$). Spectroscopically identified sources are assigned $P_i = 1$ if $z_L < z < z_U$ or else $P_i = 0$. For X-ray sources without spectroscopic redshifts we integrate the photometric redshift PDZ to determine P_i .

We then define a three dimensional observed colour-colour-magnitude space. For each source with secure spectroscopic redshift in the range $z_L < z < z_U$, we sum the probabilities P_i of all nearby X-ray sources within a colour-colour-magnitude sphere. Within the same sphere we also count the number of X-ray sources with spectroscopic redshifts in the interval $z_L < z < z_U$, N_{spec} . The weight w_i for each spectroscopic source is $\sum_i P_i / N_{\text{spec}}$. Typical weight values are 1.12 for the redshift range $0.1 < z < 0.6$ and 1.25 for the X-ray AGN in the interval $0.6 < z < 1.2$.

The XLF is estimated separately in the redshift intervals ($z_L = 0.1$, $z_U = 0.6$) and ($z_L = 0.6$, $z_U = 1.2$). The data spheres are defined by the observed $\mathcal{R} - \mathcal{I}$, $\mathcal{I} - \mathcal{K}$ colours and the \mathcal{R} -band magnitude. As in the previous section the symbols $\mathcal{R}\mathcal{I}\mathcal{K}$ are defined as MUSYC RIK for CDFS, CFHT ri and WIRC K , respectively for AEGIS-XD, SUBARU r^+i^+ and WIRCAM K_s , respectively in the case of C-COSMOS.

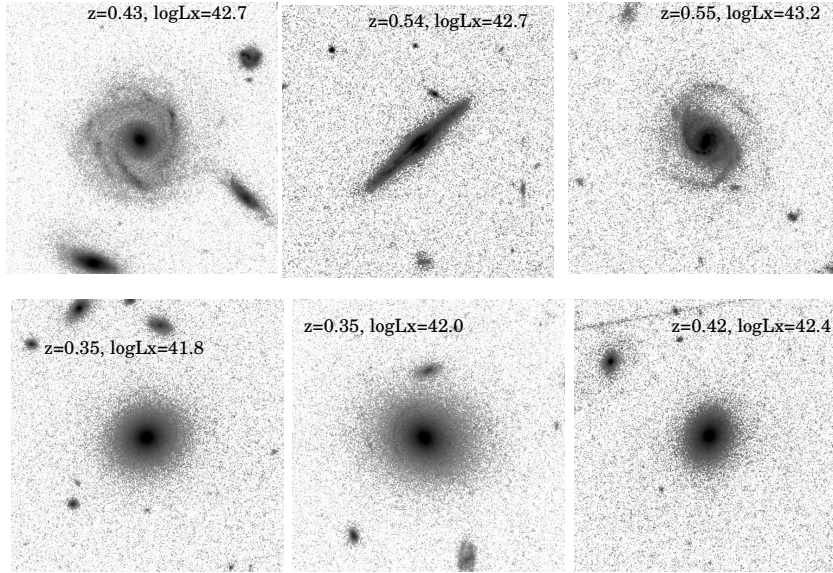


Figure 3. Examples of HST/ACS morphologies of X-ray AGN in the C-COSMOS field associated with galaxies in the quiescent (bottom row) and star-forming (top row) region of the UVJ diagram. The images are 15 arcsec on the side and have a pixel scale of 0.03 arcsec (Koekoemoer et al. 2007). The filter used in the HST/ACS survey of the COSMOS field is the F814W.

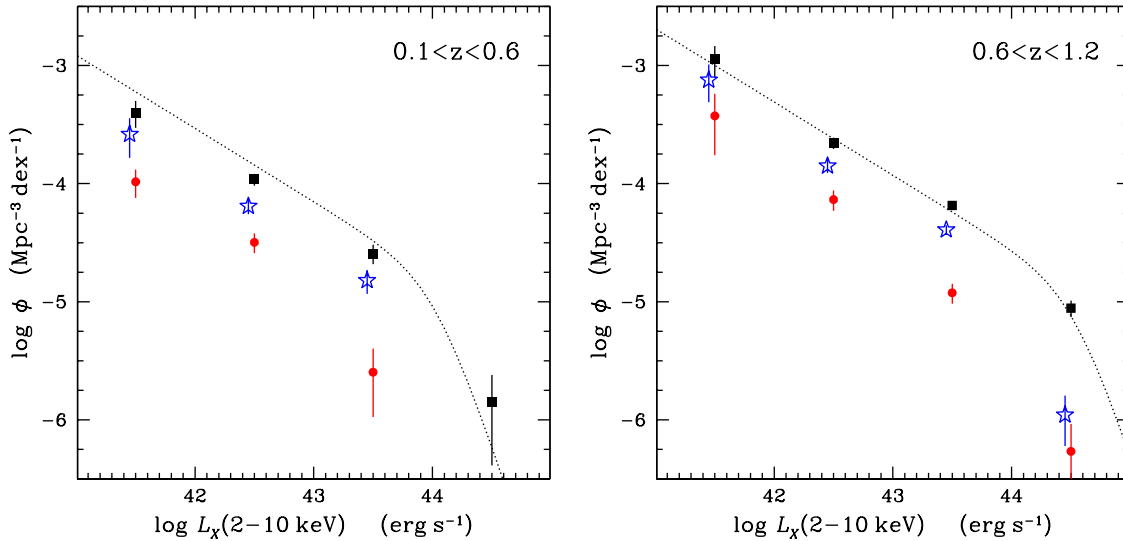


Figure 6. The 2-10 keV X-ray luminosity function. The black squares are the XLF estimates from the combined CDFS, AEGIS-XD and C-COSMOS fields in the redshift intervals $z = 0.1 - 0.6$ and $z = 0.6 - 1.2$. The dotted lines correspond to the Luminosity And Density Evolution (LADE) model of Aird et al. (2010) estimated at the median redshift of each sample. In all panels the red circles are AGN hosted by galaxies in the quiescent wedge of the UVJ diagram. Blue stars are for AGN associated with star-forming galaxies (both blue and dusty) in the UVJ diagram. Systems in which AGN emission contaminates the host galaxy colours are not plotted.

5 RESULTS

5.1 Star-formation properties of X-ray AGN hosts

Figure 2 presents the UVJ diagram of X-ray AGN in two redshift bins, 0.1–0.6 and 0.6–1.2. For comparison we also plot in the same figure the rest-frame UVJ colours of spectroscopically confirmed galaxies in the MUSYC, AEGIS-XD and C-COSMOS fields using the methodology described in section 3. The spectroscopic redshifts of the galaxy samples are from the MUSYC compilation, DEEP2,

DEEP3 (Newman et al. 2012; Cooper et al. 2011, 2012) and the VIMOS/zCOSMOS bright project (Lilly et al. 2009).

In Figure 2 quiescent systems are separated from star-forming (including dusty) galaxies by the selection wedge defined by the relations $U - V > 1.3$, $V - J < 1.6$ and $U - V > 0.88(V - J) + 0.69$ (Williams et al. 2009). The specific star-formation rate of galaxies is found to change rapidly across the wedge, at least for redshifts $z \lesssim 1.5$ (Williams et al. 2009). Some level of mixing between low and high specific star-formation rate galaxies is ex-

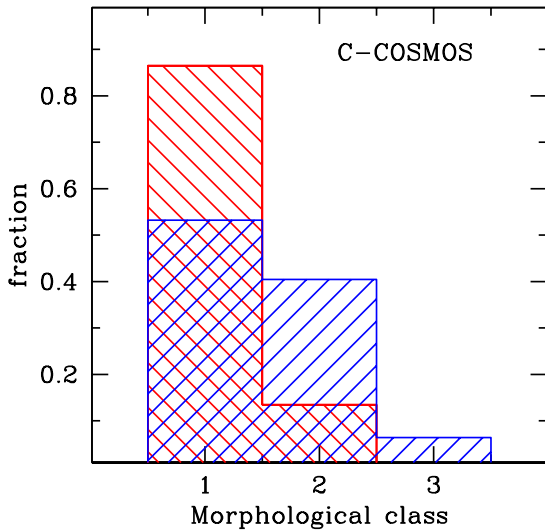


Figure 4. Morphological mix of X-ray AGN hosts in the C-COSMOS field (spectroscopic redshift interval 0.6–1.2). The sample is split into three groups, early-types, spirals and irregulars, which correspond to morphological class numbers 1, 2 and 3 respectively (Tasca et al. 2009). The red and blue histograms correspond to X-ray AGN hosts in the quiescent and star-forming region of the UVJ diagram.

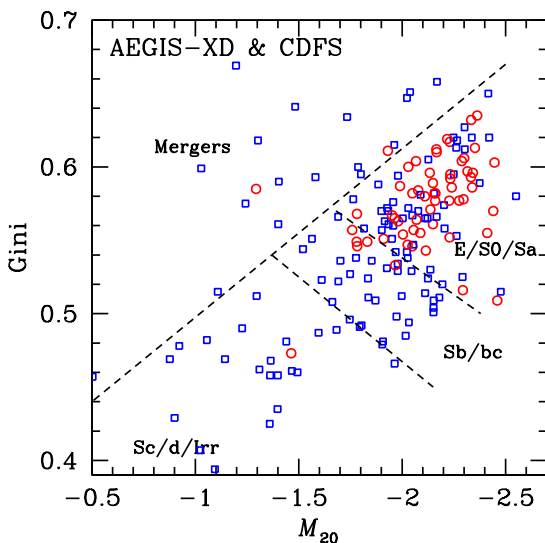


Figure 5. Gini- M_{20} diagram for X-ray AGN in the AEGIS-XD and CDFS fields (spectroscopic redshift interval 0.6–1.2) with counterparts in the HST/ACS surveys of those fields (Lotz et al. 2008; Messias 2011). The regions of the parameter space occupied by different galaxy types are demarcated with the dashed lines. Red circles and blue squares correspond to X-ray AGN hosts in the quiescent and star-forming region of the UVJ diagram respectively. The Gini and M_{20} parameters are estimated from the HST/ACS images in F814W (AEGIS-XD) and F775W (CDFS) filters

pected at the transition region of the UVJ diagram. Nevertheless, to the first approximation the UVJ colour-colour plot provides a simple diagnostic of the level of star-formation in galaxies. Turning next to X-ray AGN, they are found in galaxies in both the quiescent and the star-forming region of Figure 2. This suggests that the growth of SMBHs to $z \approx 1$ is taking place in galaxies with a wide range of star-formation histories. The apparent displacement in Figure 2 between star-forming galaxies (peak of the black contours) and X-ray AGN hosts in the star-forming part of the UVJ diagram (blue squares) is because of the different stellar mass distributions of the two populations. X-ray AGN are typically associated massive hosts, while star-forming galaxies in any magnitude-limited sample include a large fraction of low stellar mass systems.

The morphology of AGN hosts also changes across the quiescent galaxy selection wedge of Figure 2. This underlines that the distribution of X-ray AGN on the UVJ diagram reflects differences in the properties of their hosts. X-ray AGN in the quiescent wedge of the UVJ diagram are dominated by ellipticals. In contrast, X-ray AGN hosts in the star-forming part of the UVJ diagram include a large fraction of spirals. Examples of the morphologies of AGN hosts in the C-COSMOS field are presented in Figure 3. Figures 4 and 5 plot quantitative non-parametric measures of the host galaxy morphology for X-ray AGN in the C-COSMOS, AEGIS-XD and CDFS fields. In the C-COSMOS field we use the morphological catalogue of Tasca et al. (2009). They classified galaxies detected in the HST/ACS survey of the COSMOS field into early types, spirals and irregulars based on their position in the multi-dimensional space defined by the galaxies’ apparent magnitudes and three non-parametric morphological quantities, the Concentration index, the asymmetry parameter and the Gini coefficient (Abraham et al. 2003; Lotz et al. 2004). Figure 4 shows the morphological mix of X-ray AGN hosts in the C-COSMOS survey. Sources in the quiescent region of the UVJ diagram are mostly found in bulge-dominated hosts ($\approx 85\%$) and only a small fraction is associated with disks ($\approx 15\%$). In contrast X-ray AGN in the blue part of the UVJ diagram are nearly equally split between early-types and disks/irregulars. Similar results are obtained in the AEGIS-XD and CDFS fields. The morphologies of the galaxies detected in the HST/ACS surveys of those fields are quantified by the Gini coefficient and the second moment of the brightest 20% pixels of the galaxy, M_{20} (Lotz et al. 2008; Messias 2011). Different Hubble types are separated in the Gini- M_{20} diagram and the morphological classification based on these two non-parametric estimators remains robust to high redshift. Figure 5 shows that X-ray AGN hosts in the quiescent region of the UVJ diagram are distributed in the early-type region of the Gini- M_{20} parameter space. In contrast a large fraction of X-ray AGN with blue UVJ colours scatter into the late-type region of the Gini- M_{20} diagram.

The evidence above is consistent with different physical conditions of black hole growth in AGN selected on the basis of the UVJ colours of their hosts. This perhaps reflects diverse accretion modes, which can be isolated by selecting on the star-formation rate of AGN hosts. Splitting AGN samples by the level of star-formation of their hosts could therefore place limits on the significance of different fuelling modes to the accretion history of the Universe. Figure 6 for example, shows the 2–10 keV XLF of AGN in the redshift intervals $z = 0.1 - 0.6$ and $0.6 - 1.2$ split into quiescent and star-forming hosts based on their position in the UVJ diagram. The latter population dominates the space density of AGN at both redshift intervals. Nevertheless, active black holes in quiescent hosts also have a non-negligible contribution to the XLF. This result is placed into a quantitative footing by estimating for each redshift interval

the integrated X-ray luminosity density associated with AGN in quiescent and star-forming hosts based on their UVJ colours. We then normalise to the total X-ray luminosity density in each redshift bin and plot the results against look-back time and redshift in Figure 7. The accretion density is dominated by actively star-forming galaxies at redshifts 0.1–1.2. AGN in quiescent systems have a small, but non-negligible, contribution to the X-ray luminosity density, $\approx 15 - 20$ per cent. It is also interesting that within the errors, the accretion density in quiescent and star-forming galaxies does not appear to evolve strongly in the last 8 Gyrs of cosmic time.

We also caution that a fraction of the accretion density in Figure 7 is associated with X-ray sources for which the AGN light dominates the observed UV/optical continuum. For this population we have no handle on the level of star-formation of their hosts because their UVJ colours are not representative of the underlying stellar population. Studies of broad-line AGN at low redshift ($z \lesssim 0.1$) suggest that they are mostly found in star-forming hosts (Trump et al. 2013). In our work however, we prefer to keep these sources as a separate class. They are identified via the template SED fits to the observed multi-waveband photometry described in section 2. X-ray AGN that are best-fit by the AGN/galaxy hybrid templates of Salvato (2009, 2011) are marked as potentially having UVJ colours contaminated by the central AGN. Figure 2 shows that this approach identifies the majority of X-ray sources with very blue $U - V$ colours. The preference for an AGN/galaxy hybrid template by the SED fitting process correlates well with the presence of broad emission lines in the optical spectra of individual sources (Lusso et al. 2012).

5.2 Specific accretion rate

If the level of star-formation of AGN hosts traces different conditions of black hole growth, one may also expect differences in the accretion properties of the SMBH as a function of star-formation rate. It is therefore interesting to explore the Eddington ratio distribution (λ_{Edd} , observed accretion rate onto the SMBH relative to the Eddington limit) between AGN in quiescent and star-forming hosts. The Eddington ratio relates directly to properties of the active black hole and is therefore the quantity one would like to study in relevance to host galaxy properties. This exercise however, is limited by the ability to measure the mass of the black hole of individual AGN in the absence of broad optical emission lines, e.g. because of obscuration. In this case, one has to estimate first the bulge mass of the host galaxy and then assume a Magorrian-type scaling relation to approximate the mass of the central black hole. Both steps however, are not trivial and may suffer uncertainties and systematics, particularly in the case of high redshift AGN samples.

The specific accretion rate, λ , defined as the ratio between the AGN accretion luminosity and host galaxy stellar mass (Aird et al. 2012; Bongiorno et al. 2012), is advantageous because it is related to quantities that can be measured with systematic uncertainties that are typically smaller than in the case of black hole mass determinations. The specific accretion rate measures how fast a black hole grows relative to the integrated star-formation history of its host. For bulge dominated galaxies, λ is also a proxy of the Eddington ratio. The next section discusses differences between λ and λ_{Edd} .

When constructing the λ distribution of AGN there are two selection biases that need to be accounted for. The first relates to the fact that the AGN sample is optical magnitude limited, i.e. $\mathcal{R} < 24$ mag. This translates to different stellar mass limits for star-forming and quiescent hosts because of the different mass-to-light ratio of their stellar populations. This introduces incompleteness

as passive galaxies of a given stellar mass drop out of the sample at lower redshift compared to star-forming galaxies of the same stellar mass. Figure 8 demonstrates this source of bias by plotting stellar mass as a function of redshift for AGN hosts colour-coded by their position on the UVJ diagram. Quiescent hosts are scarce at low stellar masses. We minimise this source of bias by applying a redshift-dependent mass limit which corresponds to a maximally old (i.e. maximal mass-to-light ratio) galaxy. This is defined by a passively evolving stellar population that formed by an instantaneous burst at $z = 5$. We use the Bruzual & Charlot (2003) model with a Salpeter IMF to construct the evolving SED of such a stellar population and estimate at each redshift the stellar mass that corresponds to an observed magnitude of $\mathcal{R} = 24$ mag (see Fig. 8). Above this mass limit the galaxy sample is not affected by incompleteness as no galaxy should have a mass-to-light ratio greater than that of the maximally old stellar population model.

Another source of bias is related to the minimum X-ray luminosity we adopt for identifying AGN among galaxies. AGN in low stellar mass hosts are detected above the L_X limit of the sample only if they have higher specific accretion rates compared to AGN in higher stellar mass galaxies. We account for this bias by applying a minimum host galaxy stellar mass limit. This translates to a minimum specific accretion rate below which incompleteness is kicking in. We choose minimum stellar masses of $M_{star} > 10^{10} M_{\odot}$ and $> 10^{11} M_{\odot}$ for AGN at redshifts < 0.6 and > 0.6 , respectively. Figure 8 shows that this choice, in combination with the mass limit of a maximally old stellar population, result in nearly volume limited AGN samples in the redshift intervals 0.1–0.6 and 0.6–1.0. These two subsamples are used to construct and compare the specific accretion rate distributions of AGN associated with host galaxies in the quiescent and star-forming regions of the UVJ diagram. The total number of UVJ passive and star-forming AGN hosts are respectively 43, 81 ($0.1 < z < 0.6$) and 50, 91 ($0.6 < z < 1$).

The specific accretion rate is estimated as the ratio of the bolometric accretion luminosity, L_{bol} , of the AGN and the stellar mass of its host, M_* (see section 3). The L_{bol} is estimated from the X-ray luminosity in the 2–10 keV band by adopting the bolometric corrections of Marconi et al. (2004). For the construction of the specific accretion rate distributions each source i is weighted by the same factor used to estimate luminosity function, i.e. $w_i/V_{max,i}$ (see section 4). Sources in the sample for which the underlying stellar emission is contaminated by AGN light are not used in the analysis. Figure 9 plots the space density of AGN in specific accretion rate bins for the redshift intervals 0.1 – 0.6 and 0.6 – 1.0. The upper x-axis in both panels of Figure 9 shows the conversion between specific accretion rate and Eddington ratio under the assumptions of a bulge-dominated galaxy (i.e. $M_{star} = M_{bulge}$) and a bulge mass to black-hole mass scaling relation of $M_{SMBH} = 0.002 M_{bulge}$ (Marconi & Hunt 2003).

The statistical methodology based on the Kolmogorov–Smirnov test presented in the Appendix is used to compare the specific accretion rate distributions of AGN in star-forming and quiescent hosts plotted in Figure 9. We estimate a null hypothesis probability that the two samples are drawn from the same parent population of 5 and 25 per cent for AGN in the redshift intervals $0.1 < z < 0.6$ and $0.6 < z < 1.0$, respectively. The comparison is limited to specific accretion rates above the completeness limits, i.e. vertical dotted lines, of Fig. 9. We therefore find evidence, significant at the 2σ level, that low redshift AGN in star-forming/quiescent hosts have different specific accretion rate distributions. For the high redshift sub-sample however, the specific

accretion rates of AGN split by their position on the UVJ diagram are consistent.

5.3 Eddington ratio vs specific accretion rate

The specific accretion rate is a proxy of the Eddington ratio of AGN only for bulge dominated galaxies under the assumption of a scaling relation between bulge mass and black hole mass (e.g. Magorrian et al. 1998). Figures 4 and 5 however, show that about half of the star-forming X-ray AGN hosts are late-type galaxies in which the bulge mass represents a fraction of the total stellar mass. For this subsample the specific accretion rate likely underestimates the Eddington ratio.

If we were to estimate the Eddington ratios of the current X-ray AGN sample we should substitute the total stellar mass with the bulge mass of the host galaxy and adopt a Magorrian-type scaling relation (e.g. Marconi & Hunt 2003) to determine the mass of the black hole. For early-type hosts the total stellar mass is a good proxy of the bulge mass and therefore to the first approximation the Eddington ratio differs from the specific accretion rate only by a constant (i.e. upper x-axis of Fig. 9). For late-type galaxies however, there is an additional factor M_{bulge}/M_{total} , i.e. the ratio of the bulge to total stellar mass, that should also be included in the calculation. This factor would shift the Eddington ratios of X-ray AGN in late-type galaxies to higher values compared to those plotted in the upper x-axis of Figure 9. This correction could potentially alter the overall λ_{Edd} distribution of AGN in star-forming hosts relative to those in quiescent galaxies.

We explore this possibility by assuming for late-type AGN hosts $M_{bulge}/M_{total} = 0.5$, i.e. typical for Sb/Sbc-type galaxies (e.g. Fukugita et al. 1998; Oohama et al. 2009). Assuming a single M_{bulge}/M_{total} ratio is clearly an approximation. Late-type AGN hosts likely span a range of Hubble types and even within a given morphological class the bulge to total stellar mass ratio varies considerably. Nevertheless, the simplistic assumption of $M_{bulge}/M_{total} = 0.5$ for all late-type hosts illustrates the direction and amplitude of the change in the Eddington ratio distribution of AGN one should expect once more accurate black-hole mass estimates (i.e. factor of few, Shen 2013) for individual AGN become available.

The black solid line in Figure 9 shows the updated λ_{Edd} distribution of AGN in star-forming hosts assuming $M_{bulge}/M_{total} = 0.5$ for the late-type sub-population and $M_{bulge}/M_{total} = 1$ for early-types. For the construction of those distributions we account for the fact that the AEGIS-XD and CDFS fields have only partial HST/ACS coverage. For those fields we only consider the subregion with HST/ACS data. The total number of star-forming AGN hosts with HST/ACS data in the redshift intervals $0.1 < z < 0.6$ and $0.6 < z < 1.0$ are 80 and 87, respectively. As expected, the overall impact of using variable M_{bulge}/M_{total} to approximate the black hole mass of galaxies with different morphologies is a shift to higher Eddington ratios of AGN in star-forming hosts. The net effect is an increase of their space density at $\log \lambda_{Edd} \gtrsim -2$ relative to AGN in quiescent galaxies.

We assess differences in the Eddington ratio distributions plotted in Figure 9 (black and red histograms) using the methodology presented in the Appendix. We estimate a null hypothesis probability that the two distributions are drawn from the same parent population of 6 and 23 per cent for AGN in the redshift intervals $0.1-0.6$ and $0.6-1.0$, respectively. Therefore, for the low redshift subsample we extended to the Eddington ratio the results of the previous section on the specific accretion rate. We find tentative evidence,

significant at the 2σ level, that AGN in star-forming and quiescent galaxies have different Eddington ratio distributions. At higher redshift, $0.6 < z < 1.0$, we find no evidence for a difference in the accretion properties of AGN split by UVJ colours. For that subsample however, if we limit the comparison to $\log \lambda_{Edd} \gtrsim -3$ we estimate a null hypothesis probability of 2 per cent that the two distributions are drawn from the sample parent population. There is therefore evidence, significant at the $\approx 2\sigma$ level, that the accretion properties of AGN in the range $0.6 < z < 1.0$ and with $\log \lambda_{Edd} \gtrsim -3$ depend on the level of star-formation of their hosts.

6 DISCUSSION

We combine Chandra data in the CDFS, AEGIS and C-COSMOS fields with UV-to-near-IR photometry to place X-ray AGN hosts on the UVJ diagram and split them into quiescent and star-forming systems independent of dust induced biases. Morphological evidence further suggests that grouping AGN hosts by their UVJ colour selects black holes that grow their mass under different physical conditions related to different levels of star-formation rate.

We then estimate the fraction of the accretion density of the Universe associated with high/low specific star-formation rate AGN hosts in the redshift range $0.1-1.2$. It is found that most of the supermassive black hole growth at those redshifts is associated with galaxies in the high specific star-formation rate region of the UVJ diagram. Figure 8 suggests that this result may be a selection effect of the optical magnitude limit $\mathcal{R} = 24$ mag applied to the X-ray AGN samples. Nevertheless, we estimate a total XLF in Figure 6 that agrees well with the results of Aird et al. (2010). This indicates that if we miss AGN because of the optical magnitude limit of the sample, their contribution to the space density and hence, the integrated X-ray luminosity density, should be small.

Also, our finding that the accretion density is dominated by AGN in star-forming galaxies is consistent with studies that link the growth of SMBHs to the specific star-formation of their hosts. Georgakakis et al. (2011) showed that the evolution with redshift of the optical and stellar-mass functions of AGN hosts relative to the overall galaxy population suggests that they are associated with high specific star-formation rate systems. In this picture the rapid decline of the AGN space density at $z < 1$ is related to the drop of the average specific star-formation rate of the overall galaxy population at those redshifts. Herschel data also suggest that AGN hosts have, on average, specific star-formation rates similar to or even higher than galaxies on the main star-formation sequence (e.g. Santini et al. 2012; Rovilos et al. 2012). Clustering studies that attempt to constrain the distribution of AGN in the cosmic web and not just their mean dark matter halos mass, find that a potentially large fraction of the population at $z \lesssim 1$ lives in $\log M/M_{\odot} \approx 12-13$ halos (Allevato et al. 2012; Mountrichas et al. 2013). This is close to the characteristic dark matter halo mass scale where the efficiency of star-formation peaks, in terms of stellar mass over dark matter halo mass ratio (e.g. Moster et al. 2010; Leauthaud et al. 2012; Behroozi et al. 2013).

At the same time however, we also find that a fraction of X-ray AGN are associated with early-type hosts in the quiescent, low specific star-formation rate region of the UVJ diagram. This is consistent with studies that use the alternative approach of fitting model templates to the observed spectral energy distribution to account for dust reddening (Cardamone et al. 2010b).

We also explore whether active SMBHs split by the UVJ colour of their hosts have different accretion properties, which

would suggest different fueling modes. We estimate the specific accretion rate, λ , of X-ray AGN to approximate the accretion properties of the central black hole. We also convert λ into approximate Eddington ratios, λ_{Edd} , by assuming a correlation between black hole mass and bulge stellar mass. For the low redshift sub-sample of Fig. 9 we find evidence, significant at the 2σ level, that X-ray AGN in star-forming and quiescent hosts have different specific accretion rate or Eddington ratio distributions. AGN in star-forming hosts dominate at high λ or λ_{Edd} , while those in quiescent hosts become increasingly important toward low Eddington ratios or specific accretion rates. We do not find such trends for AGN in the interval $0.6 < z < 1.0$. At those redshifts the specific accretion rate distributions of AGN split by the level of star-formation of their hosts are consistent. However, there is evidence significant at the 2σ level that the Eddington ratio distribution of the subsample with $\log \lambda_{Edd} \gtrsim -3$ is different for *UVJ* selected star-forming and quiescent AGN hosts. Differences at a similar significance level in the specific accretion rate distributions of obscured AGN at $z = 0.6 - 4$ split by the level of star-formation of their hosts was reported previously by Brusa et al. (2009).

The evidence above tentatively suggests the presence of different fuelling modes among the X-ray AGN population at least out to $z \approx 0.6$. If confirmed with larger samples, this would extend to higher redshifts results from local samples ($z \lesssim 0.1$), which report striking differences at a high statistical significance level in the accretion properties of SDSS narrow optical emission-line AGN as function of the level of star-formation of their hosts (Kauffmann & Heckman 2009). It is shown that active black holes associated with the most actively star-forming galaxies dominate at high Eddington ratios and follow a log-normal distribution in λ_{Edd} . In contrast, active SMBHs in quiescent galaxies are characterised by low Eddington ratios and a power-law distribution in λ_{Edd} .

The less pronounced trends between specific accretion rate and star-formation in our sample compared to the results of Kauffmann & Heckman (2009) likely relate to differences in the analysis of the data and ultimately, observational limitations (e.g. signal-to-noise ratio, number statistics) when performing population studies of AGN outside the local Universe. We use broad-band rest-frame colours as a proxy to star-formation rate and split X-ray AGN into two groups, star-forming and quiescent. In reality however, AGN hosts span a range of star-formation rates. Kauffmann & Heckman (2009) find that the Eddington ratio distribution of AGN in their sample varies smoothly from log-normal for the subsamples with the highest level of star-formation to power-law toward the least star-forming hosts. This trend is diluted when splitting into broad bins of star-formation. Another difference between the results presented here and those of Kauffmann & Heckman (2009) is the method adopted to approximate the mass of the black hole and hence, determine the corresponding Eddington ratio. We use the total stellar mass as proxy of the bulge mass and therefore estimate the specific accretion rate instead of the Eddington ratio of AGN. We attempt to correct, at least in an approximate way, for the fact that the bulge mass of some AGN hosts are only a fraction of the total stellar mass. Nevertheless, the lack of bulge mass proxies (e.g. bulge/disk decomposition, stellar velocity dispersion) for individual sources in the sample could further dilutes any trends between Eddington ratio and star-formation rate.

GALFORM is one of the semi-analytic model for the cosmological evolution of AGN and galaxies that postulates two channels of black hole growth, each of which occurs in galaxies with distinct star-formation histories (Bower et al. 2006; Fanidakis et al. 2012). In that SAM SMBHs grow when their hosts experience a

starburst event, because of either secular processes (e.g. disk instabilities) or mergers. A fraction of the gas that is available to star-formation is assumed to accrete onto the SMBH. Additionally, in GALFORM AGN activity is also triggered when diffuse hot gas in quasi-hydrostatic equilibrium in the parent dark matter halo is accreted onto the SMBH without being cooled first onto the galactic disk. The latter fuelling mode is decoupled from star-formation and occurs in passive galaxies. The evolution of the AGN population in GALFORM is related to the interplay between the two SMBH fuelling modes. The starburst channel is important at high redshift and high accretion rates, while the hot halo accretion mode dominates at low redshifts and low accretion rates. Moreover, the Eddington ratio distribution in GALFORM is bimodal as a result of the two fuelling modes (see Figure 1 of Fanidakis et al. 2013). The starburst mode dominates at accretion rates close to Eddington and has a tail that extends to low Eddington ratios. The hot-halo model becomes important at low accretion rates relative to the Eddington limit. There are therefore similarities, at least at the qualitative level, between the accretion properties of AGN in GALFORM and those inferred in the present paper or from local samples (Kauffmann & Heckman 2009).

A prediction of GALFORM is that a fraction of the accretion density of the Universe at a given redshift is associated with passive low specific-star-formation galaxies. This is tested in Figure 7, which compares the observational data with the predictions of GALFORM. AGN hosts in that model are first split into star-forming and quiescent using the same *UVJ* selection wedge adopted for the real data. The 2-10 keV X-ray luminosity function of the two sub-populations is then integrated to determine their fractional contribution to the total accretion density. The results are plotted as a function of redshift in Figure 7. In the comparison of the model with the data we attempt to account for the fraction of broad-line AGN in the observations. Although there are suggestions that such systems are mostly found in star-forming hosts at low redshift ($z \lesssim 0.1$; Trump et al. 2013), it is challenging to constrain the *UVJ* colours of the underlying stellar population of the higher redshift broad-line AGN sample presented here. We therefore choose to correct the model predictions for this population. From the observations we estimate at any given X-ray luminosity and redshift interval the space density of the AGN with contaminated colours relative to the total XLF, $f_{QSO}(L_X, z)$. This fraction is then subtracted from the GALFORM model XLF when integrating to determine the starburst and hot-halo mode luminosity densities relative to the total.

GALFORM predicts that the contributions of the hot-halo and starburst modes to the accretion density change rapidly and in opposite directions with redshift, i.e. see inset plot of Figure 7. This trend, although diluted, is still present even after correcting the model results for the observed fraction of BL QSOs in the sample (i.e. main panel of Figure 7). Another prediction of GALFORM is that about 30% of the X-ray luminosity density at both $z = 0.40$ and $z = 0.85$ is associated with AGN in quiescent hosts accreting in hot-halo mode. These predictions are in tension with the observational results plotted in Figure 7. We find that only up to 20% of the X-ray luminosity density at $z \lesssim 1$ is associated with AGN hosts in the quiescent region of the *UVJ* diagram. Also the fraction of the accretion density associated with star-forming/quiescent hosts does not change within the errors from $z = 0.85$ to $z = 0.40$. One possible solution to these discrepancies is to relax the tight correspondence between accretion mode and host galaxy *UVJ* colours in GALFORM. Hot-halo mode AGN hosts in that model do not form new stars and are therefore found predominantly in the quiescent part of the *UVJ* diagram. In contrast, starburst mode AGN hosts

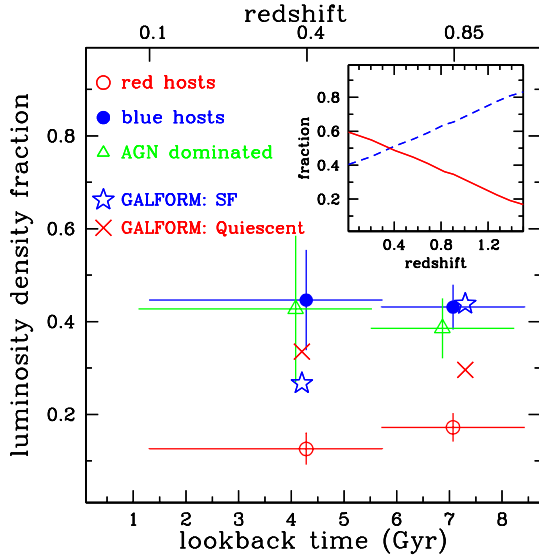


Figure 7. The fraction of the X-ray luminosity density associated with different AGN samples is plotted as a function of look-back time (lower x-axis) and redshift (upper x-axis). The red open circles are for red AGN hosts, the blue filled circles represent AGN in blue hosts and the green triangles correspond to AGN with optical colours contaminated by the central engine. The vertical errorbars are Poisson estimates propagated from the uncertainties in the X-ray luminosity density. The horizontal errors represent the redshift interval of the different sub-samples. For clarity the triangles are offset by -0.2 Gyrs. The inset plot shows as a function of redshift the predictions of GALFORM SAM for the fractional contribution to the total X-ray luminosity density of AGN in *UVJ*-quiescent (red solid line) and *UVJ*-star-forming (blue dashed curve) hosts. These results cannot be directly compared with the observations because of the fraction of broad-line QSOs in the sample for which host galaxy colours cannot be determined. We therefore correct GALFORM predictions at redshifts $z = 0.4$ and $z = 0.85$ for the observed fraction of broad-line QSOs in the sample as described in the text. These corrected model predictions are plotted with the blue stars (AGN hosts in the star-forming region of the *UVJ* diagram) and red crosses (AGN hosts in the quiescent region of the *UVJ* diagram).

populate almost exclusively the star-forming region of the *UVJ* diagram. The assumption of the model that hot-halo mode AGN are completely disjoint from star-formation is probably conservative. Some level of star-formation might be expected in the hosts of those AGN as the hot gas cools from galactic scales onto the black hole. Allowing for this effect could shift a fraction of the hot-halo AGN in GALFORM into the blue region of the *UVJ* diagram. In this respect it is important that GALFORM predicts a sufficiently large pool of hot-halo AGN, which could populate the red region of the *UVJ* diagram.

7 CONCLUSIONS

We use the *UVJ* diagram to split AGN hosts into star-forming (including dust reddened) and quiescent. The host-galaxy morphology of the two sub-populations is found to be different, suggesting that selection on the *UVJ* diagram provides a means of identifying SMBHs that grow their mass under distinct physical conditions. AGN hosts in the quiescent region of the *UVJ* diagram are early-type bulge dominated galaxies. In contrast, star-forming AGN hosts include a large fraction (about 50%) of late-type systems. We also

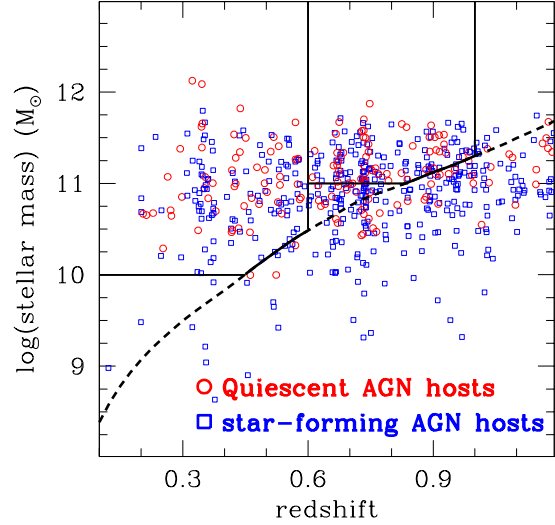


Figure 8. X-ray AGN host galaxy stellar mass as a function of redshift. Red circles and blue squares are for AGN hosts in the quiescent and star-forming region of the *UVJ* diagram, respectively. The black dashed curve shows the redshift-dependent mass limit of a maximally old galaxy with $\mathcal{R} = 24$ mag (see text for details). The horizontal solid lines show the mass limits of 10^{10} and $10^{11} M_{\odot}$, used to define nearly volume-limited AGN samples in the redshift intervals $z = 0.1 - 0.6$ and $0.6 - 1.0$. The vertical solid lines mark the limits of those redshift intervals. AGN within the wedges defined by the continuous sections of the black dashed curve and the vertical and horizontal solid lines are used to construct specific accretion rate distributions.

estimate the fraction of the accretion density associated with those two classes of hosts at redshifts $z \approx 0.40$ and 0.85 . Most of the accretion density at those redshifts is taking place in star-forming hosts. Nevertheless, about 15-20% of the AGN luminosity density is associated with galaxies in the quiescent part of the *UVJ* diagram. There is also evidence, significant at the 2σ level, that AGN in the low redshift subsample ($0.1 < z < 0.6$) have accretion properties that depend on the level of star-formation of their hosts. AGN in star-forming hosts dominate at high Eddington ratios, while those in quiescent hosts become increasingly important toward low Eddington ratios. At higher redshift, $0.6 < z < 1.0$, such differences are present at the 2σ level only for AGN with Eddington ratios $\log \lambda_{Edd} \gtrsim -3$. These results are consistent with two modes for growing black holes that take place in galaxies with different star-formation properties. We compare those observations with the predictions of GALFORM SAM, which postulates two black hole growth channels, one linked to star-formation and the other occurring in passive systems. This SAM predicts a fraction of accretion density in quiescent hosts that is larger than the observed. We also find that the evolution with redshift of the X-ray luminosity density of hot-halo/starburst mode AGN is inconsistent with the observations. We argue that these discrepancies could be attributed to the assumption of GALFORM that the hot-halo accretion mode is not accompanied with some level of star-formation in the host galaxy. Relaxing this requirement could bring the model in better agreement with the data.

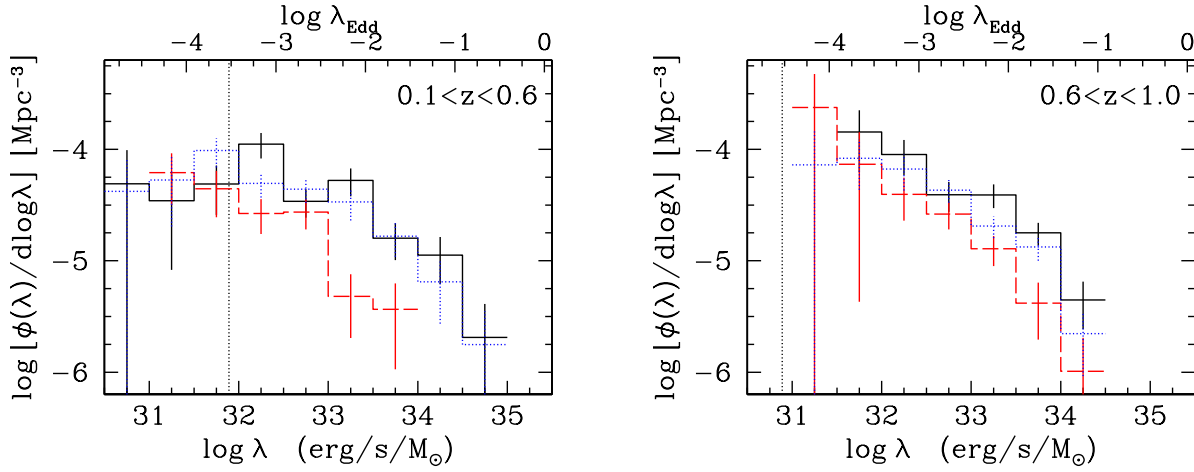


Figure 9. Specific accretion rate distribution, λ of X-ray AGN in quiescent (red dashed histogram) and star-forming (blue dotted histogram) hosts, classified on the basis of their UVJ colours. The panel on the left corresponds to X-ray AGN in the redshift interval 0.1–0.6. The panel on the right is for X-ray AGN in the redshift range $z = 0.6 - 1.0$. The vertical dotted line shows the specific accretion rate completeness limits for the two samples, i.e. $\log \lambda \gtrsim 32$ and $\log \lambda \gtrsim 31$ ($\text{erg/s}/M_{\odot}$) for the $z = 0.1 - 0.6$ and $z = 0.6 - 1.0$ samples respectively. The y-axis in both panels is space density in logarithmic bins of specific accretion rate. The top y-axis shows the correspondence between specific accretion rate and Eddington ratio, λ_{Edd} under the assumptions that AGN hosts are bulge-dominated (i.e. bulge mass, M_{bulge} , equals the total stellar mass of the galaxy) and black hole mass scales with bulge mass as $M_{SMBH} = 0.002 M_{bulge}$ (Marconi & Hunt 2003). The former assumption breaks down for late-type AGN hosts in the star-forming region of the UVJ diagram (e.g. Fig. 4, 5), for which the bulge mass is fraction of the total stellar mass. The Eddington ratio of those AGN is underestimated by a factor equal to the ratio of the bulge to total stellar mass ratio, M_{bulge}/M_{total} . The black solid histogram plots how the λ_{Edd} distribution of AGN in star-forming hosts changes if we assume $M_{bulge}/M_{total} = 0.5$ for the late-type sub-population and $M_{bulge}/M_{total} = 1$ for early-types.

8 ACKNOWLEDGMENTS

The authors wish to thank the referee, M. Brusa, for providing constructive comments and suggestions. PGP-G acknowledges support from the Spanish Programa Nacional de Astronomía y Astrofísica under grant AYA2012-31277. This work has made use of the Rainbow Cosmological Surveys Database, which is operated by the Universidad Complutense de Madrid (UCM), partnered with the University of California Observatories at Santa Cruz (UCO/Lick,UCSC). Funding for the DEEP2 Galaxy Redshift Survey has been provided in part by NSF grants AST95-09298, AST-0071048, AST-0071198, AST-0507428, and AST-0507483 as well as NASA LTSA grant NNG04GC89G. Funding for the DEEP3 Galaxy Redshift Survey has been provided by NSF grants AST-0808133, AST-0807630, and AST-0806732. This work benefited from the THALES project 383549 that is jointly funded by the European Union and the Greek Government in the framework of the programme “Education and lifelong learning”.

REFERENCES

- Abraham R. G., van den Bergh S., Nair P., 2003, *ApJ*, 588, 218
Aird J., Coil A. L., Moustakas J., Blanton M. R., Burles S. M., Cool R. J., Eisenstein D. J., Smith M. S. M., Wong K. C., Zhu G., 2012, *ApJ*, 746, 90
Aird J., et al., 2010, *MNRAS*, 401, 2531
Allevato V., et al., 2011, *ArXiv* 1105.0520
—, 2012, *ApJ*, 758, 47
Barro G., Pérez-González P. G., Gallejo J., Ashby M. L. N., Kajisawa M., Miyazaki S., Villar V., Yamada T., Zamorano J., 2011a, *ApJS*, 193, 13
—, 2011b, *ApJS*, 193, 30
Behroozi P. S., Wechsler R. H., Conroy C., 2013, *ApJ*, 762, L31
Bessell M. S., 1990, *PASP*, 102, 1181
Blanton M. R., Roweis S., 2007, *AJ*, 133, 734
Bongiorno A., et al., 2012, *MNRAS*, 427, 3103
Bower R. G., Benson A. J., Malbon R., Helly J. C., Frenk C. S., Baugh C. M., Cole S., Lacey C. G., 2006, *MNRAS*, 370, 645
Brusa M., et al., 2009, *A&A*, 507, 1277
—, 2010, *ApJ*, 716, 348
Bruzual G., Charlot S., 2003, *MNRAS*, 344, 1000
Bundy K., Ellis R. S., Conselice C. J., Taylor J. E., Cooper M. C., Willmer C. N. A., Weiner B. J., Coil A. L., Noeske K. G., Eisenhardt P. R. M., 2006, *ApJ*, 651, 120
Calzetti D., Armus L., Bohlin R. C., Kinney A. L., Koornneef J., Storchi-Bergmann T., 2000, *ApJ*, 533, 682
Capak P., et al., 2007, *ApJS*, 172, 99
Cardamone C. N., Urry C. M., Schawinski K., Treister E., Brammer G., Gawiser E., 2010a, *ApJ*, 721, L38
—, 2010b, *ApJ*, 721, L38
Cisternas M., et al., 2011, *ApJ*, 726, 57
Coil A. L., Georgakakis A., Newman J. A., Cooper M. C., Croton D., Davis M., Koo D. C., Laird E. S., Nandra K., Weiner B. J., Willmer C. N. A., Yan R., 2009, *ApJ*, 701, 1484
Cooper M. C., et al., 2011, *ApJS*, 193, 14
—, 2012, *MNRAS*, 419, 3018
Elvis M., et al., 2009, *ApJS*, 184, 158
Fanidakis N., Baugh C. M., Benson A. J., Bower R. G., Cole S., Done C., Frenk C. S., Hickox R. C., Lacey C., Del P. Lagos C., 2012, *MNRAS*, 419, 2797
Fanidakis N., et al., 2013, *ArXiv e-prints* 1305.2200
Fioc M., Rocca-Volmerange B., 1997, *A&A*, 326, 950
Fukugita M., Hogan C. J., Peebles P. J. E., 1998, *ApJ*, 503, 518
Georgakakis A., Rowan-Robinson M., Babbedge T. S. R., Georgantopoulos I., 2007, *MNRAS*, 377, 203
Georgakakis A., et al., 2009, *MNRAS*, 397, 623

—, 2011, *MNRAS*, 418, 2590
 Giavalisco M., et al., 2004, *ApJ*, 600, L93
 Hickox R. C., et al., 2009, *ApJ*, 696, 891
 Hopkins A. M., Beacom J. F., 2006, *ApJ*, 651, 142
 Hutchings J. B., Frenette D., Hanisch R., Mo J., Dumont P. J., Redding D. C., Neff S. G., 2002, *AJ*, 123, 2936
 Kauffmann G., Heckman T. M., 2009, *MNRAS*, 397, 135
 Kelly B. C., Merloni A., 2012, *Advances in Astronomy*, 2012
 Kocevski D. D., et al., 2012, *ApJ*, 744, 148
 Koekomoer A. M., et al., 2007, *ApJS*, 172, 196
 Kormendy J., Ho L. C., 2013, *ARA&A*, 51, 511
 Laird E. S., et al., 2009, *ApJS*, 180, 102
 Leauthaud A., et al., 2012, *ApJ*, 744, 159
 Lilly S. J., et al., 2009, *ApJS*, 184, 218
 Lin H., Yee H. K. C., Carlberg R. G., Morris S. L., Sawicki M., Patton D. R., Wirth G., Shepherd C. W., 1999, *ApJ*, 518, 533
 Lotz J. M., Primack J., Madau P., 2004, *AJ*, 128, 163
 Lotz J. M., et al., 2008, *ApJ*, 672, 177
 Lusso E., et al., 2012, *MNRAS*, 425, 623
 Magorrian J., Tremaine S., Richstone D., Bender R., Bower G., Dressler A., Faber S. M., Gebhardt K., Green R., Grillmair C., Kormendy J., Lauer T., 1998, *AJ*, 115, 2285
 Marconi A., Hunt L. K., 2003, *ApJ*, 589, L21
 Marconi A., Risaliti G., Gilli R., Hunt L. K., Maiolino R., Salvati M., 2004, *MNRAS*, 351, 169
 McCracken H. J., et al., 2010, *ApJ*, 708, 202
 Messias H., 2011, PhD thesis, University of Lisbon
 Mignoli M., et al., 2004, *A&A*, 418, 827
 Morrison R., McCammon D., 1983, *ApJ*, 270, 119
 Moster B. P., Somerville R. S., Maulbetsch C., van den Bosch F. C., Macciò A. V., Naab T., Oser L., 2010, *ApJ*, 710, 903
 Mountrichas G., Georgakakis A., 2012, *MNRAS*, 420, 514
 Mountrichas G., Georgakakis A., Finoguenov A., Erfanianfar G., Cooper M. C., Coil A. L., Laird E. S., Nandra K., Newman J. A., 2013, *MNRAS*, 430, 661
 Mullaney J. R., et al., 2012, *MNRAS*, 419, 95
 Nandra K., Pounds K. A., 1994, *MNRAS*, 268, 405
 Newman J. A., et al., 2012, *ArXiv e-prints*, 1203.3192
 Oohama N., Okamura S., Fukugita M., Yasuda N., Nakamura O., 2009, *ApJ*, 705, 245
 Patel S. G., Holden B. P., Kelson D. D., Franx M., van der Wel A., Illingworth G. D., 2012, *ApJ*, 748, L27
 Pérez-González P. G., et al., 2008, *ApJ*, 675, 234
 Rosario D. J., et al., 2012, *A&A*, 545, A45
 —, 2013, *ArXiv e-prints* 1302.1202
 Rovilos E., et al., 2012, *A&A*, 546, A58
 Salvato M., et al., 2011, *ApJ*, 742, 61
 Sanders D. B., et al., 2007, *ApJS*, 172, 86
 Santini P., et al., 2012, *A&A*, 540, A109
 Schmidt M., 1968, *ApJ*, 151, 393
 Shen Y., 2013, *Bulletin of the Astronomical Society of India*, 41, 61
 Sutherland W., Saunders W., 1992, *MNRAS*, 259, 413
 Tasca L. A. M., et al., 2009, *A&A*, 503, 379
 Trump J. R., Hsu A. D., Fang J. J., Faber S. M., Koo D. C., Kocevski D. D., 2013, *ApJ*, 763, 133
 Trump J. R., et al., 2009, *ApJ*, 696, 1195
 Williams R. J., Quadri R. F., Franx M., van Dokkum P., Labbé I., 2009, *ApJ*, 691, 1879
 Willmer C. N. A., et al., 2006, *ApJ*, 647, 853
 Xue Y. Q., et al., 2011, *ApJS*, 195, 10

APPENDIX A: STATISTICAL COMPARISON OF ACCRETION RATE DISTRIBUTION OF AGN SAMPLES

This section describes the methodology followed to assess differences in the specific accretion rate distribution of AGN in quiescent and star-forming hosts. We use the Kolmogorov–Smirnov (K-S) test to estimate the probability of the null hypothesis that the two distributions are drawn from the same parent population.

The K-S test cannot be used to compare directly the space density distribution of AGN in specific accretion rate bins plotted in Figure 9. This is because those distributions are constructed by normalising each source in the sample by V_{max} (see section 4), i.e. correcting for the selection function. Also, it is not possible to apply the K-S test to the “observed” specific accretion rate distributions, i.e. those constructed by summing up AGN without applying any V_{max} corrections. This is because small differences in the selection functions of AGN in quiescent and star-forming hosts, e.g. X-ray luminosity distribution, could bias any results.

The approach we follow instead starts with a model for the space density of AGN as a function of specific accretion rate for one of the two samples we wish to compare, for example AGN in star-forming hosts. This is then convolved with the selection function of the second sample, i.e. in this example AGN in quiescent hosts. The resulting model distribution can then be compared to the “observed” specific accretion rate distribution of AGN in quiescent hosts using the K-S test. The underlying assumption is that the two samples, quiescent and star-forming, are drawn from the same parent population.

We choose as model for the space density of AGN as a function of accretion rate, $\phi(\lambda)$, the one inferred from observations (i.e. Figure 9). The selection function of each sample, quiescent or star-forming, is essentially encapsulated in the V_{max} estimated for individual sources. To the first approximation we can therefore use those discrete values to account for selection effects. Figure A1 shows that V_{max} is a function of specific accretion rate, in the sense that lower specific accretion rate systems have, on average, smaller V_{max} , i.e. they drop from the sample at lower redshift, compared to higher accretion rate systems.

The convolution of $\phi(\lambda)$ with the selection function proceeds as follows. First we sample from $\phi(\lambda)$ to produce a series of λ values. The AGN from the real sample catalogue with specific accretion rate closest to each of the random λ draws is identified. The V_{max} corresponding to that AGN is assigned to the λ randomly drawn from $\phi(\lambda)$. This V_{max} value is then used to determine if the corresponding λ should be retained in the sample. A random number in the range $0 - 1$ is produced and is compared with the ratio $V_{max}/max(V_{max})$, where $max(V_{max})$ is the maximum of all V_{max} in the sample. If the random number is less than $V_{max}/max(V_{max})$ then λ is kept, otherwise it is discarded. These steps are repeated for all λ values drawn from the model $\phi(\lambda)$. The retained λ values are used to build the cumulative probability distribution function of the model. The K-S test is then applied to compare the distribution of specific accretion rates drawn from the model after convolving with the selection function with that inferred from the observations without applying any V_{max} corrections to individual sources.

As an example, we compare the specific accretion rate distribution of AGN in quiescent/star-forming hosts in the redshift interval $z = 0.1 - 0.6$ plotted in 9-left. We only consider sources with $\log \lambda > 32$ ($\text{erg/s}/M_{\text{dot}}$). At lower specific accretion rates incompleteness is affecting the estimated space density of AGN. We use as model the inferred $\phi(\lambda)$ for AGN in star-forming hosts plot-

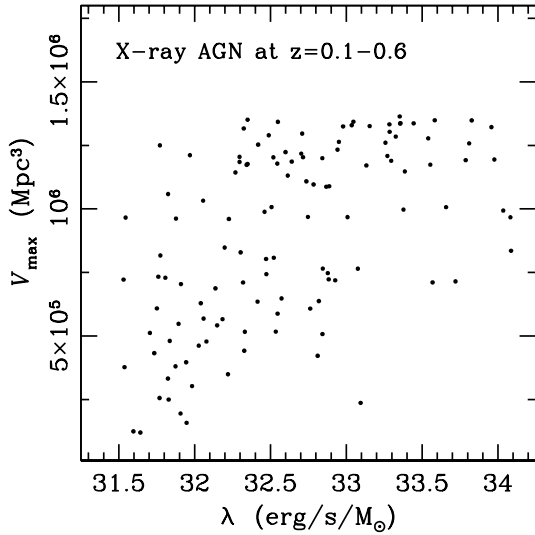


Figure A1. Maximum volume, V_{max} as a function of specific accretion rate, λ , of X-ray AGN in the redshift interval 0.1–0.6.

ted in Fig. 9-left. This is then convolved with the selection function of the quiescent AGN host. The resulting cumulative distribution for AGN in star-forming hosts is plotted in Figure A2. Also plotted is that figure is the “observed” cumulative distribution of AGN in quiescent hosts. The K-S test is used to estimate the probability that the two distributions are drawn from same parent population. The null hypothesis has a probability of 5 per cent. Therefore, in the redshift interval $z = 0.1 - 0.6$ AGN in quiescent/star-forming hosts have different specific accretion rate distributions at the 95 per cent confidence level, or about 2.0σ in the case of a Normal distribution.

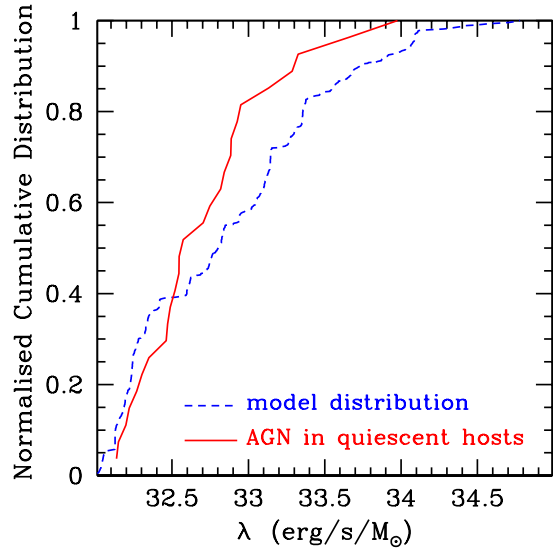


Figure A2. Normalised cumulative distribution of AGN as a function of specific accretion rate, λ . The red solid curve is for AGN in quiescent hosts in the redshift interval 0.1–0.6. This is constructed by summing up sources without applying any selection function corrections. The blue dashed distribution is the comparison sample constructed from the space density of AGN in star-forming hosts and convolving with the selection function of the AGN in quiescent hosts (see text for details). The K-S test can be applied to those distributions to estimate the null hypothesis that the two populations are drawn from the same parent population.